Received 15 May 2023; Accepted 7 August 2023
https://doi.org/10.22226/2410-3535-2023-4-329-334

Check for updates

Orientation-dependent evolution of the microstructure in polycrystalline cooper deformed by tension

N. Y. Zolotorevsky[†,1,2], V. V. Rybin[1,2], E. A. Ushanova[1,2,3], V. N. Perevezentsev[2]

[†]zolotorevsky@phmf.spbstu.ru

[1]Institute of Physics and Mechanics, Peter the Great Polytechnic University, St-Petersburg, 195251, Russia
[2]Mechanical Engineering Research Institute of the RAS, Nizhny Novgorod, 603024, Russia
[3]CRISM "Prometey" — National Research Center "Kurchatov Institute", St. Petersburg, 191015, Russia

Abstract: The microstructure has been analyzed using the EBSD technique in two locations of the neck region of the cooper tensile specimen, the local true strains in which were estimated as 0.45 and 1.15. It was shown that the orientation-dependent evolution of the microstructure occurs concurrently with the development of the crystallographic texture. Grains oriented in the [111] corner of the stereographic triangle accumulate a high density of extended low-angle boundaries delineating cell blocks, but keep a relatively uniform orientation of the tensile direction. Inside grains oriented in the [100] corner, the density of cell block boundaries is significantly lower. Nevertheless, the latter grains lose their uniform orientation, which is accompanied by the appearance of deformation fragments having high-angle boundaries. These peculiarities of the microstructure evolution are discussed in terms of polycrystal micromechanics.

Keywords: copper, plastic deformation, microstructure, texture, EBSD

1. Introduction

Various microstructures are formed within the interior of grains during plastic deformation of polycrystals, in particular, original grains are gradually subdivided into regions (cell blocks, fragments), whose dislocation boundaries evolve from low to high misorientation angles [1–6]. Such boundaries are often regarded as geometrically necessary (GNBs) since they separate regions with different slip systems activity [7].

It has been found that the microstructure depends on the crystallographic orientation of grains, inside which it is formed [8–17]. This effect was studied extensively on the example of rolling because of its practical importance [8,9,12–15]. At the same time, the FCC metals deformed in tension turned out to be a suitable object of study due to the formation of the simple fiber texture with two components, <111> and <100>. It has been established by TEM that the microstructures of aluminum and copper observed after true strains from 0.05 to ≈0.3 could be grouped into three types, and a correspondence between the microstructure type and the grain orientation has been found [18–22]. It is of interest, however, to investigate how the orientation effect manifests itself at larger strains, at the stage of grain fragmentation [2–6]. Indeed, a challenging scientific problem, which arises when trying to describe the simultaneous evolution of microstructure and crystallographic texture, is the interrelation between the grain fragmentation and the texture development [23]. Many attempts have been made to find a way to solve this problem [24–31], including the approaches based on self-consistent viscoplastic [25,26,29] and crystal plasticity [30,31] simulation. However, there is no currently quantitative theory of this kind, in particular, due to a lack of experimental data regarding the orientation effect on the development of fragmented microstructure. In order to fill this gap, in the present research the microstructure was examined within the neck region of the copper tensile sample. It allowed us to study true strains well above those achievable at the stage of uniform deformation.

2. Materials and methods

The material used was commercially pure copper (99.9% purity). A cylindrical specimen with 35 mm gauge length and 5 mm diameter was tensile strained at room temperature until fracture (Fig. 1a), at a strain rate of $3 \cdot 10^{-2}$ s^{-1}. For the following examination, the necked specimen has been cut

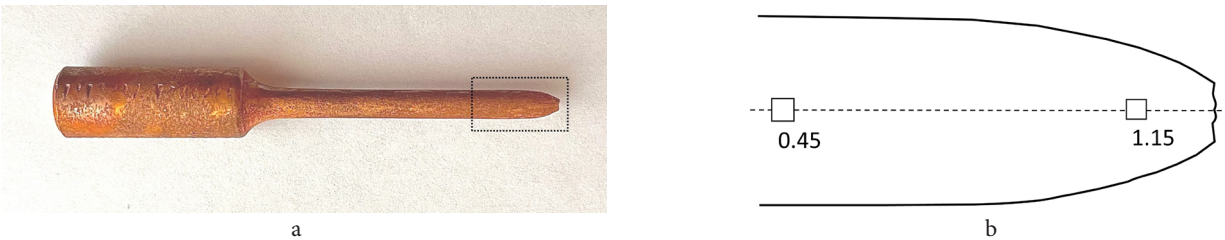

a b

Fig. 1. (Color online) Half of the copper tensile specimen deformed until fracture (a) and schematic drawing of its longitudinal section with two examined regions indicated by boxes (b).

along the tensile direction (TD). Regions for the EBSD analysis were chosen in two places on the longitudinal section near the central axis of the specimen (Fig. 1b). The strains analysis [32] and FE modelling [33] showed that the local plastic strain in the region around the specimen axis is approximately equal to the average strain in a given cross-section of the specimen. With this in mind, local true strains were estimated from the local diameter D using the equation $\varepsilon = 2\log(D_0 / D)$, where D_0 is the initial diameter of the specimen. True strains thus obtained for the mapped regions were 0.45 and 1.15. The EBSD analysis was carried out on SEM LYRA 3 XMN RL using Oxford HKL AZtec™ software on the areas $\approx 300 \times 300$ μm² with scanning steps of 250 and 200 nm for strains 0.45 and 1.15, respectively. The raw indexing rate of the EBSD data was over 85% in each case. The orientation maps were subjected to clean-up procedure. The processing of the data was performed by means of MTEX software [34], in particular, the techniques of half-quadric minimization was used to denoise orientation maps.

3. Results

The undeformed material had a weak texture with a slight concentration of TD pole density near the [111] corner of stereographic triangle (Fig. 2); the grain size determined by the linear intercept method with taking twin boundaries into account was about 30 μm. The microstructures formed during tension are shown in Fig. 3 together with corresponding textures. A comparison with the initial condition shows, in particular, that strong <111>+<100> fiber texture develops already at the strain of 0.45. The area fraction of the <100> fiber, meanwhile, remains approximately equal to the initial one (Fig. 4). Hence, it may be suggested that most grains, which first had unstable orientations, reorient to <111>, whereas the second fiber is created mainly from those grains that had orientations close enough to <100>. In what follows, grains oriented in the [100] and [111] corners of stereographic triangle will be referred to as the [100] and [111] type grains, respectively. One can notice on the EBSD maps shown in Fig. 3b that orientation non-uniformity develops primarily in the [100] type grains. This non-uniformity manifests itself both in the appearance of coarse grain-scale domains and in the formation of small highly misoriented fragments located mainly near original grain boundaries.

Figure 5 shows more closely the deformation microstructures of grains oriented in different corners of stereographic triangle. Here, in order to reveal in more detail the substructure, we, first, lowered to 1° the minimal angle for boundary visualization and, second, considered the KAM (kernel average misorientation) maps. The latter parameter is a measure of local misorientation, calculated as the average of misorientations between a given point and its nearest neighbors. When calculating KAM, only misorientations less than 5° were included, and only the first nearest neighbors

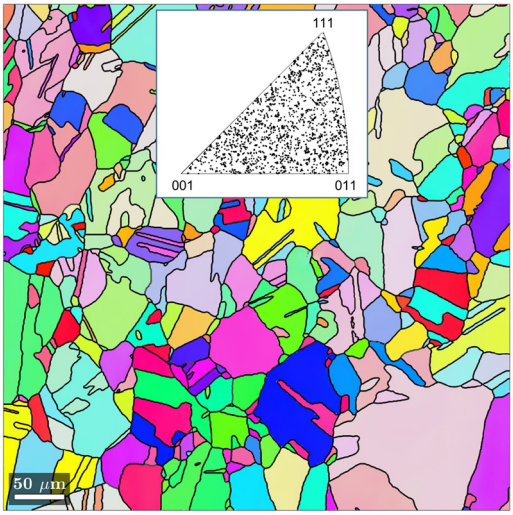

Fig. 2. (Color online) Initial microstructure of copper together with the discrete IPF showing the distribution of TD on the standard stereographic triangle.

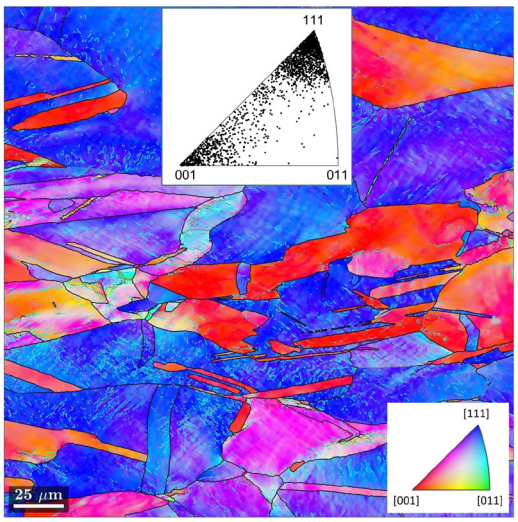

a

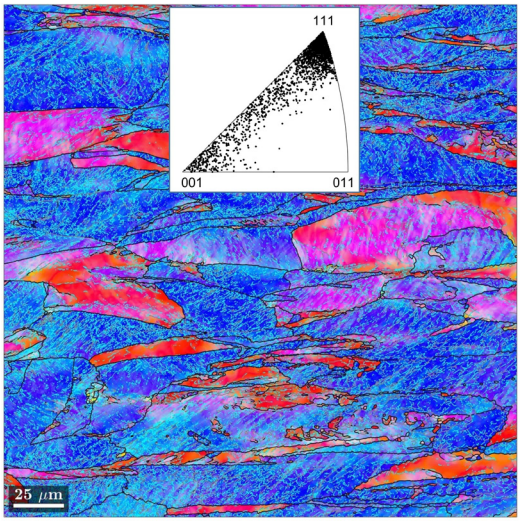

b

Fig. 3. (Color online) Microstructures of copper deformed to strains 0.45 (a) and 1.15 (b) together with the discrete IPFs showing the distribution of TD (directed horizontally) on the standard stereographic triangle. The orientation maps are the inverse pole figure (IPF) maps plotted with respect to TD. Correspondence between boundary color and angle (θ) of misorientation: 2°< θ < 5°, cyan; 5°< θ <15°, grey; θ >15°, black. The color-coding of the maps is shown on the stereographic triangle.

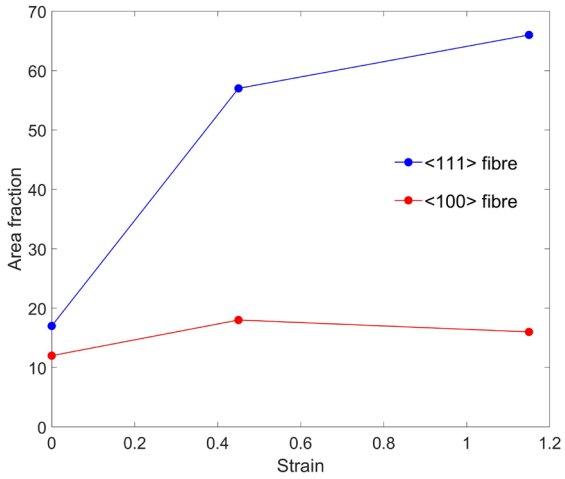

Fig. 4. (Color online) Area fractions of fiber texture components derived from orientation maps with a tolerance deviation of 15° from ideal orientations.

(four points in the case of square grid) were taken into account. It should be emphasized that so defined KAM is used in the present study not for highlighting regions of different curvature, but in order to visualize subboundaries or cell walls with misorientations even lower than 1°.

Examples of the microstructure formed at $\varepsilon = 0.45$ are shown in Fig. 5 a, b. Subboundaries with misorientations exceeding 1° are almost absent in the [100] type grain presented in Fig. 5 a. Moreover, the submicron cell structure, which was well observed by TEM [18 – 20], is almost invisible inside this grain even on the KAM map. This is evidence of (i) the absence of cell block boundaries and (ii) the low level of misorientation between cells, which is consistent with the Type 2 structure observed at smaller strains [18 – 20]. Inside the grain deviated a little more from [100], Fig. 5 b, the extended subboundaries occur with misorientations up to ≈2.5°, parallel to the {111} plane, confirming the alignment of cell block boundaries similar to those of the Type 1 structure [19]. Alternatively, two sets of intersecting extended dislocation boundaries occur inside the [111] type grains observed in Figs. 5 a, b, which is consistent with the Type 3 structure [19]. Therefore, the correlation between the type of microstructure and the grain orientation previously established in copper for smaller strains by TEM, remains largely at the strain of 0.45.

With increasing strain, the above noted differences in the microstructure become even more prominent, Figs. 5 c, d. In particular, the systematic substructure with the high density of cell block boundaries develops inside the [111] type grains, whereas such a cell block structure is degenerated inside the [100] ones. The latter are characterized rather by the dislocation boundaries extended along the TD, as one can see Fig. 5 c. Note, however, that large [100] domains similar to those presented in Figs. 5 c are not typical for $\varepsilon = 1.15$. Instead, the [100] type grains are generally subdivided into highly misoriented fragments, Figs. 5 d.

In order to characterize the orientation effects quantitatively, those grains (the "grains" were reconstructed with the tolerance of 15°), whose mean orientations deviate by less than 15° from [100]||TD, will be further assigned to the [100] type, while those with deviations of less than 15° from [111]||TD — to the [111] one. Figure 6 shows the misorientation angle distributions for these two groups of grains in terms of boundary length per unit area (the line graphs were drawn based on histograms determined with a bin width of 1°). One can see that the boundary length in the [111] type grains is considerably larger than in the [100] type ones for relatively low angles, but inverse relation occurs for higher angles. With increasing strain, the overall

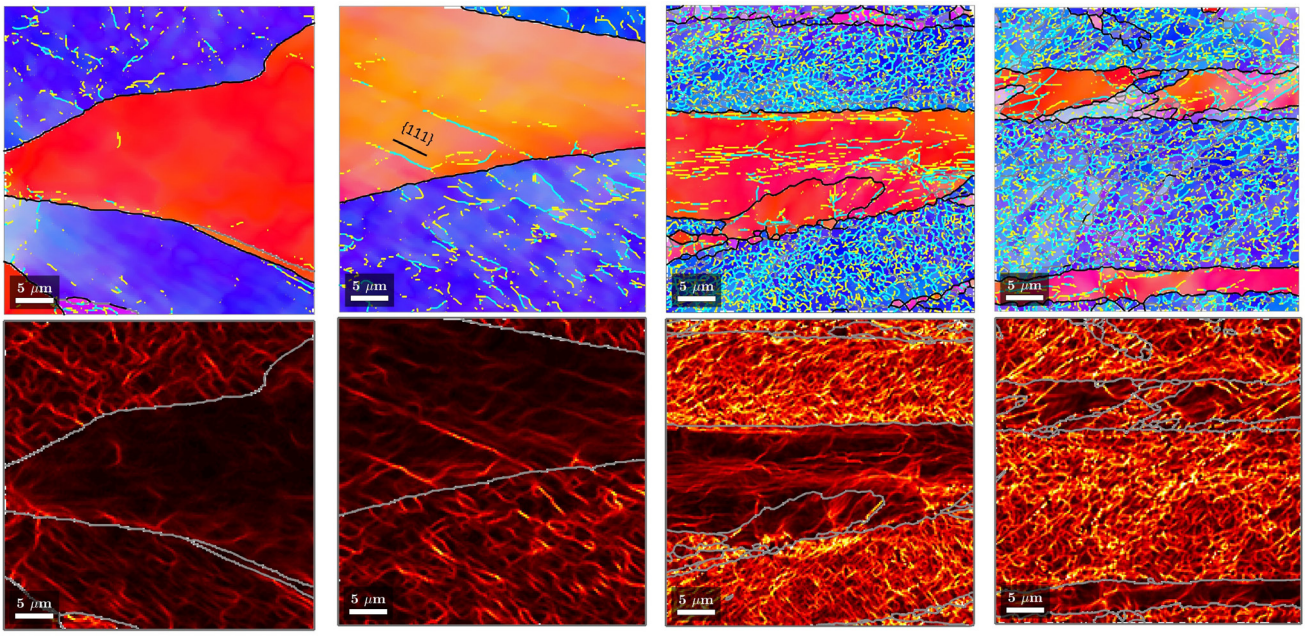

Fig. 5. (Color online) Orientation maps (the upper level) and KAM (the lower level) maps illustrating a correlation between microstructure peculiarities and crystal orientation at strains 0.45 (a, b) and 1.15 (c, d). The orientation maps are the IPF maps plotted with respect to TD, which is directed horizontally. Color-coding of boundaries on the IPF maps: $1° < \theta < 2°$, yellow; $2° < \theta < 5°$, cyan; $5° < \theta < 15°$, grey; $\theta > 15°$, black. On the KAM maps, grains reconstructed with a 5° tolerance angle are outlined by thin light grey boundaries.

length of strain-induced boundaries per unit area increases about fivefold, however, the previous relations remain. This confirms, in particular, that highly misoriented fragments arise in the [100] type grains with greater probability than in the [111] type ones.

Another orientation effect concerns the axes of misorientation across the strain-induced boundaries. At $\varepsilon = 0.45$, the axes are predominantly perpendicular to the TD in the grains of both types (Fig. 6a). This is quite expected if (i) slip systems with the maximum resolved shear stress dominate in most grains, and (ii) strain-induced subboundaries are formed predominantly from the dislocations of these systems. However, this regularity is violated at a strain of 1.15, namely, the axes of misorientation become mostly parallel to the TD in the [111] type grains (Fig. 6b). Therefore, despite the fact that the GNBs form inside these grains due to spatial variations of slip system activity, the operating slip patterns ensure the preservation of TD orientation.

The above considered peculiarities of the microstructure evolution determine the fact that strongly fragmented regions have orientations primarily in the [100] corner or in the middle part of the stereographic triangle. To quantify this observation, the grains/fragments reconstructed with the tolerance of 15° have been divided into three groups according to their sizes: <5 μm, from 5 to 25 μm, and >25 μm. Figure 7 shows the distributions of grain mean orientations separately for each group. One can see that, indeed, orientations of small grains have a propensity to the [100] corner, whereas the largest grains are concentrated near the [111] corner.

4. Discussion

Analysis of the microstructure of tensile strained copper showed that its evolution occurs in essentially different ways depending on which fiber <100> or <111> the grain belongs to. Obviously, these differences are caused by the orientation dependent peculiarities of operating slip systems. Indeed, the [100] type grains are geometrically soft while the [111] type ones are hard; their Taylor factors are, respectively, 2.65 and 3.67. The softness of [100] grains leads to a relatively low dislocation density and, correspondingly, weak strain hardening [20, 35]. Moreover, the tension along [100] activates a combination of eight slip systems oriented for easy cross slip, which additionally reduces dislocation density, and also lessens the tendency to form GNBs [22].

The peculiarities mentioned above help to understand the occurrence of different microstructure types observed in copper and aluminum at small strains [20 – 22]. However, they cannot explain differences in the character of fragmentation under further straining found in the present study. Notice in this regard that at least six solutions to the Taylor ambiguity problem are possible for orientations of TD close to the [100] corner, and corresponding slip patterns produce the same strain, while creating different lattice rotations

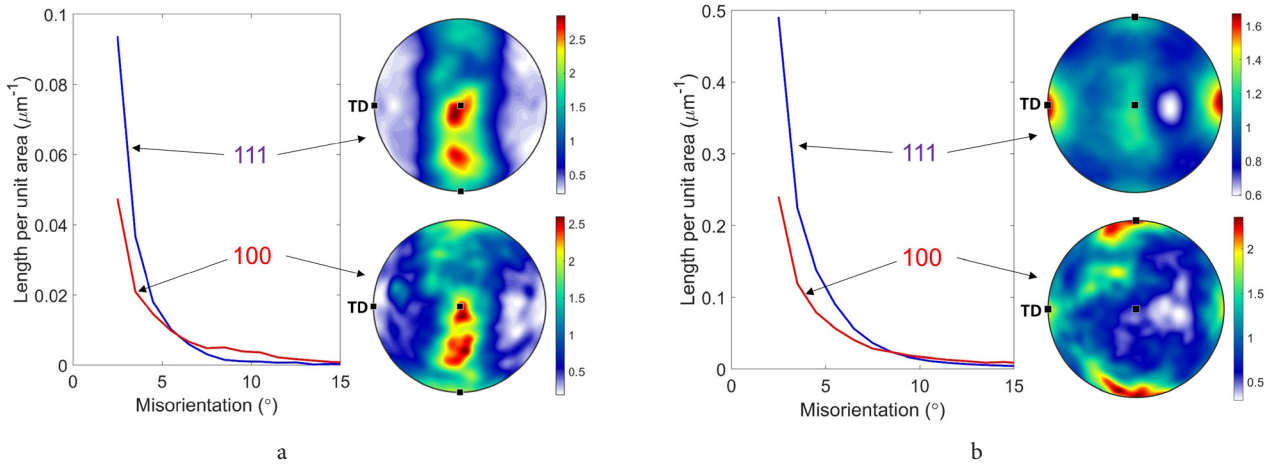

Fig. 6. (Color online) Misorientation angle distributions together with misorientation axis distributions in the sample system of coordinates inside [111] and [100] type grains for strains of 0.45 (a) and 1.15 (b).

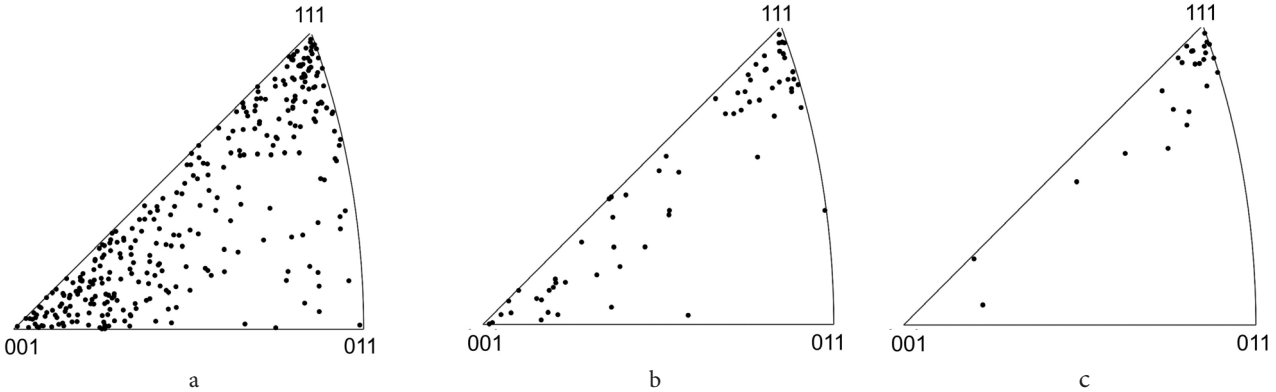

Fig. 7. TD inverse pole figures obtained for grains of different sizes: <5 μm (a), from 5 to 25 μm (b) and >25 μm (c) in case of the strain of 1.15.

[10]. The analysis of grain reorientation in polycrystalline copper deformed by tension to a strain of ≈0.25 showed that lattice rotations within coarse domains of original grains are consistent with the Taylor solutions [36]. Similar large domains having diffuse boundaries are observed in Fig. 4 a, predominantly inside [100] type grains, and hence their formation can indeed be associated with the operation of slip patterns predicted by the full-constraint Taylor model. Nevertheless, the nature of highly misoriented fragments, which occur commonly near original grain boundaries, cannot be understood in the framework of Taylor ambiguity problem. Both theoretical [37 – 39] and experimental [36, 40] investigations have demonstrated that the grain interaction plays a determining role in this phenomenon. In the case of tensile deformation of copper, this interaction, as might be expected, manifests itself in the following way. Two kinds of grains appear already at an early stage of deformation, hard [111] type grains and soft [100] type ones. The softness of the latter grains, as noted above, leads to their relatively weak strain hardening, consistent with the present observation. One can thus suppose that the [100] type grains adjust main portion of the plastic incompatibility arising between them and their [111] type neighbors. The accommodative strain inside the grain is inevitably non-uniform [28] and, correspondingly, some regions adjacent to the grain boundaries have to experience different lattice rotations. The natural results of such a grain interaction are the appearance of highly misoriented fragments within the [100] type grains. At the same time, the fine-scale fragmentation of another kind occurs inside [111] type grains, where the systematic cell block microstructure with the extended GNBs forms throughout the entire volume. Similar microstructure has been shown to evolve in single crystals of [111] orientation [10]. Therefore, the fragmentation of this kind is caused by "internal factors", namely, by the orientation dependent peculiarities of slip system partitioning. Its evolution, which includes the gradual increase of misorientation across GNDs as well as the development of microshear bands [4] or S-bands [41], also results in the formation of high-angle boundaries. However, it occurs under the plastic strains that far exceed those achieved in the present investigation [2 – 4, 41].

5. Summary

Our EBSD analysis indicates that the character of microstructure evolution in tensile strained copper depends significantly on the grain orientation. The length per unit area of the cell block boundaries with relatively low misorientation angles (less than 6 – 8°) is much larger in the [111] type grains than in the [100] ones. At the same time, the [111] type grains mostly keep uniform orientation of TD, whereas the [100] ones become subdivided into highly misoriented fragments. It was suggested that the fragmentation of [100] type grains is the mechanism, by which they adjust plastic incompatibility between them and their harder [111] neighbors.

Acknowledgements: *Financial support from the Russian Science Foundation (project No 21-19-00366) is gratefully acknowledged.*

References

1. J. G. Sevillano. Flow Stress and Work Hardening. In: Materials Science and Technology (ed. by R. W. Cahn, P. Haasen, E. J. Kramer). Wiley (2006). Crossref
2. V. V. Rybin. Large plastic deformations and fracture of metals. Metallurgiya, Moscow (1986) 224 p. (in Russian)
3. D. A. Hughes, N. Hansen. Acta Mater. 45, 3871 (1997). Crossref
4. P. J. Hurley, F. J. Humphreys. Acta Mater. 51, 1087 (2003). Crossref
5. Y. Estrin, A. Vinogradov. Acta Mater. 61, 782 (2013). Crossref
6. N. Yu. Zolotorevsky, V. V. Rybin, A. N. Matvienko, E. A. Ushanova, S. A. Philippov. Materials Characterization. 147, 184 (2019). Crossref
7. D. Kuhlmann-Wilsdorf, N. Hansen. Scr. Metall. Mater. 25, 1557 (1991). Crossref
8. Yu. Perlovich, H. J. Bunge, M. Isaenkova. Textures and Microstructures. 29, 241 (1997).
9. Q. Liu, D. Juul Jensen, N. Hansen. Acta Mater. 46, 5819 (1998). Crossref
10. N. Hansen, X. Huang, W. Pantleon, G. Winther. Phil. Mag. 86, 3981 (2006). Crossref
11. T. Ungar, A. D. Stoica, G. Tichy, X.-L. Wang. Acta Mater. 66, 251 (2014). Crossref
12. C. C. Merriman, D. P. Field, P. Trivedi. Mater. Sci. and Eng. A. 494, 28 (2008). Crossref
13. B. Bacroix, S. Queyreau, D. Chaubet, E. Siv, Th. Chauveau. Acta Materialia. 160,121 (2018). Crossref
14. H. Pirgazi, L. A. I. Kestens. Materials Characterization. 171, 110752 (2021). Crossref
15. A. Dolzhenko, M. Tikhonova, R. Kaibyshev, A. Belyakov. Metals. 12, 454 (2022). Crossref
16. A. Arya, S. Suwas, C. Gérard, L. Signor, L. Thilly, A. H. Chokshi. Acta Materialia. 221, 117396 (2021). Crossref
17. J. Baton, W. Geslin, C. Moussa. Materials Characterization. 171, 110789 (2021). Crossref
18. X. Huang, N. Hansen. Scripta Mater. 37, 1 (1997). Crossref
19. X. Huang. Scr. Mater. 38, 1697 (1998). Crossref
20. X. Huang, A. Borrego, W. Pantleon. Mater. Sci. and Eng. A. 319–321, 237 (2001). Crossref
21. X. Huang, G. Winther. Phil. Mag. 87, 5189 (2007). Crossref
22. G. Winther, X. Huang. Phil. Mag. 87, 5215 (2007). Crossref
23. E. Aernoudt, P. V. Houtte, T. Leffers. Deformation and Textures of Metals at Large Strain. In: Materials Science and Technology (ed. by R. W. Cahn, P. Haasen, E. J. Kramer). Wiley (2006). Crossref
24. M. Seefeldt, L. Delannay, B. Peeters, E. Aernoudt, P. Van Houtte. Acta Mater. 49, 2129 (2001). Crossref
25. I. J. Beyerlein, R. A. Lebensohn, C. N. Tomé. Mater. Sci. and Eng. A. 345, 122 (2003). Crossref
26. A. A. Nazarov, N. A. Enikeev, A. E. Romanov, T. S. Orlova, I. V. Alexandrov, I. J. Beyerline, R. Z. Valiev. Acta Materialia. 54, 985 (2006).
27. L. S. Toth, Y. Estrin, R. Lapovok, C. Gu. Acta Mater. 58, 1782 (2010). Crossref

28. A. Zisman. Int. J. of Eng. Science. 116, 155 (2017). Crossref
29. R. Wang, C. Lu, K. A. Tieu, A. A. Gazder. Journal of Materials Research and Technology. 18, 508 (2022). Crossref
30. K. Sedighiani, K. Traka, F. Roters, J. Sietsma, D. Raabe, M. Diehl. Acta Materialia. 237, 118167 (2022). Crossref
31. A. Arya, S. Suwas, A. H. Chokshi. Materials Science and Engineering A. 856, 143955 (2022). Crossref
32. P. J. Noell, J. E. C. Sabisch, D. L. Medlin, B. L. Boyce. Acta Mater. 184, 211 (2020). Crossref
33. M. Kuroda, A. Uenishi, H. Yoshida, A. Igarashi. Int. Journal of Solids and Structures. 43, 4465 (2006). Crossref
34. F. Bachmann, R. Hielscher, H. Schaeben. Ultramicroscopy. 111, 1720 (2011). Crossref
35. R. Wang, A. A. Saleh, G. Casillas, C. Lu, A. A. Gazder. Mater. Sci. and Eng. A. 819, 141184 (2021). Crossref
36. C. Thorning, M. A. J. Somers, J. A. Wert. Mater. Sci. Eng. A. 397, 215 (2005). Crossref
37. V. V. Rybin, A. A. Zisman, N. Yu. Zolotorevsky. Acta Metall. Mater. 41, 2211 (1993).
38. L. Delannay, O. V. Mishin, D. Juul Jensen, P. Van Houtte. Acta Mater. 49, 2441 (2001). Crossref
39. A. Ma, F. Roters, D. Raabe. Acta Mater. 54, 2181 (2006). Crossref
40. D. P. Field, A. Alankar. Metall. Mater. Trans. A. 42A, 676 (2011). Crossref
41. D. A. Hughes, N. Hansen. Acta Mater. 48, 2985 (2000). Crossref